applied sciences

MDPI

Article

A Polarization-Dependent Frequency-Selective Metamaterial Absorber with Multiple Absorption Peaks

Guangsheng Deng, Tianyu Xia, Yong Fang, Jun Yang and Zhiping Yin *

Academy of Photoelectric Technology, Hefei University of Technology, Key Lab of Special Display Technology, Ministry of Education, No. 193, Tunxi Road, Hefei 230009, China; dgsh@hfut.edu.cn (G.D.); tyxia2000@outlook.com (T.X.); fy9903@hfut.edu.cn (Y.F.); junyang@hfut.edu.cn (J.Y.)

* Correspondence: zpyin@ustc.edu; Tel.: +86-551-6290-2791

Academic Editor: Kenneth Chau

Received: 19 April 2017; Accepted: 31 May 2017; Published: 4 June 2017

Abstract: A polarization-dependent, frequency-selective metamaterial (MM) absorber based on a single-layer patterned resonant structure intended for F frequency band is proposed. The design, fabrication, and measurement for the proposed absorber are presented. The absorber's absorption properties at resonant frequencies have unique characteristics of a single-band, dual-band, or triple-band absorption for different polarization of the incident wave. The calculated surface current distributions and power loss distribution provide further understanding of physical mechanism of resonance absorption. Moreover, a high absorption for a wide range of TE-polarized oblique incidence was achieved. Hence, the MM structure realized on a highly flexible polyimide film, makingthe absorber suitable for conformal geometry applications. The proposed absorber has great potential in the development of polarization detectors and polarizers.

Keywords: absorber; metamaterial; multi-band absorption; polarization-dependent

1. Introduction

Electromagnetic metamaterials, which represent a class of artificial structures whose electric and magnetic response can be controlled freely, have attracted a significant amount of attention [1–3]. Due to their unique benefits, metamaterials have provided many important effects, such as invisible cloaking [4], negative refractive index [5], and super-lens [6].

Since the metamaterial absorber (MA) was presented in 2008 by Landy et al. [7], metamaterial has attracted many researchers because of its advantages, such as size minimization and suitable thickness, for applications using electromagnetic wave absorbers [8–10]. In recent years, various structures, such as split rings [11], closed rings [12], and fishnet structures [13], have been proposed for MAs. A certain progress has been made in broadband MAs developing [14,15]. Meanwhile, some studies on tunable absorbers [16,17] and multiband absorbers [18–20] have been performed. Currently, research is focused on absorbers intended for application in polarization imaging and polarization detecting. Therefore, the polarization-dependent frequency-selective absorbers are highly demanded. For most single patterned resonant structures, the number of absorption peaks was fixed or the absorbers were polarization-independent [21,22]. Hokmabadi et al. proposed a stereometamaterial perfect absorber, wherein absorption frequency is related to polarization angles [23]. Hu et al. presented a polarization-dependent MA with different resonant frequencies in two orthogonal directions [24]. However, these structures have only one polarization-dependent absorption peak, which limits their application in spectroscopic imaging and detecting, wherein multiple absorption peaks are required [25,26].

In this paper, the focus is on the F frequency band (F-band), and a simple polarization- dependent frequency-selective metamaterial absorber is proposed. The proposed structure has three separate absorption peaks with high absorption for TE-polarized and TM-polarized normal incident waves. Furthermore, the absorption peaks can be dynamically controlled by adjusting of a polarization angle of the incident wave. Compared to the previously reported MAs, the MA proposed in this paper has several advantages. Firstly, compared to complex resonance structures with multiple absorption peaks, such as all-in-one packed super-unit cell [27,28] and stacked layers [29], the proposed absorber has only one patterned resonant structure, which meets current demands on miniaturization and simplification. Secondly, the multiple absorption peaks can be dynamically tuned by changing of polarization angles of the incident wave. Lastly, the proposed MA structure is realized on a highly flexible polyimide film without a rigid substrate, so the absorber can be easily used in the non-planar and conformal-geometry applications.

2. Structure and Design

The proposed MA structure and the unit cell structure of the copper pattern are presented in Figure 1. Unlike previously reported results, where multiple different-sized metal patterns were used to obtain multi-band absorption, here, the simple etching of a C-shaped slot into a circular patch, provides a triple-band absorption. The geometrical dimensions of the copper pattern shown in Figure 1b are a = 820 µm, d = 60 µm, r_1 = 112.5 µm, r_2 = 161 µm, and r_3 = 367.5 µm. The copper pattern with a thickness of 0.5 µm and an electric conductivity of (5.8×10^7) S/m was printed on the top layer of a thick dielectric substrate with a thickness of 50 µm that was made of polyimide film with a relative permittivity of 3.6 and a dielectric loss tangent of 0.02. Moreover, a thick copper plate that acts as a ground plane was printed on the bottom of the dielectric substrate.

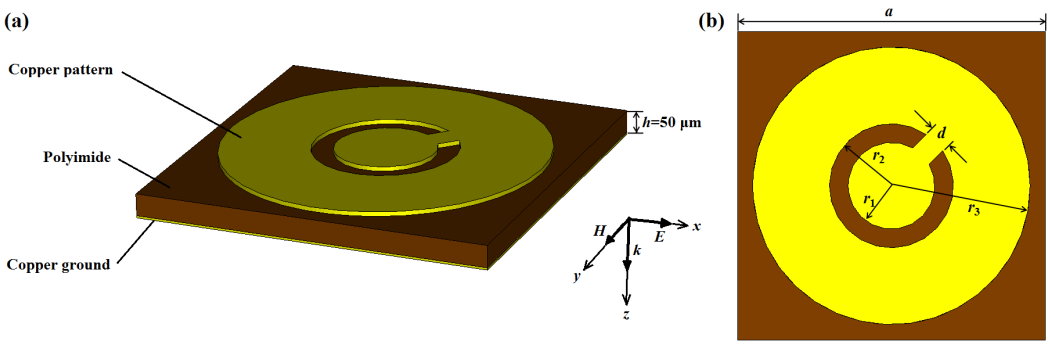

Figure 1. (**a**) The proposed metamaterial absorber (MA) unit cell structure; (**b**) layout of the unit cell structure and its optimal values given in micrometers: a = 820, d = 60, r_1 = 112.5, r_2 = 161, and r_3 = 367.5.

The absorptivity can be calculated by

$$A = 1 - |S_{11}|^2 - |S_{21}|^2 \quad (1)$$

where A, S_{11}, and S_{21} are the absorptivity, the reflection coefficient, and the transmission coefficient, respectively. In this case, the transmission coefficient S_{21} is zero because the thickness of the metal ground plane is much larger than its skin depth, so the absorptivity is determined by $A = 1 - |S_{11}|^2$.

3. Simulated Results and Discussion

The simulations were conducted in CST Microwave Studio 2014 (Darmstadt, Germany), using the finite-element frequency-domain method, and the unit cell boundary conditions were utilized in both x and y directions. Meanwhile, the Floquet port condition was employed in the z-direction. Since the proposed absorber has similar absorption characteristics for TE-polarized and TM-polarized

normal incident waves, only the electromagnetic responses for the TE-polarized incident wave, whose electric field is parallel to the x-axis, were calculated for the normal incidence angle. Three distinct absorption peaks, which are at 92.4 GHz, 102.0 GHz, and 130.1 GHz with absorptivities of 88.1%, 98.2%, and 94.6%, respectively, are presented in Figure 2. In addition, three resonance peaks were labeled as mode f_1, mode f_2, and mode f_3 starting from low to high frequencies. From Figure 2, the separation of the first two adjacent resonant peaks of the MA is not high enough, which may hinder its applications in the multiband detection. This can be improved by reconstructing the geometries of the proposed structure.

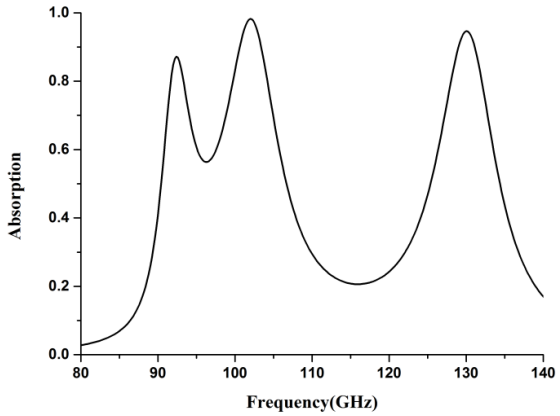

Figure 2. Absorption spectra of the proposed metamaterial absorber for the TE-polarized normal incident wave.

In order to show the intrinsic mechanism of the proposed metamaterial absorber, the surface currents distributed on the metal pattern and the metal ground plane that correspond to three absorption peaks were calculated and the obtained results are presented in Figure 3.

As shown in Figure 3a, for mode f_1, the surface currents on the metal pattern diverge from inner circular patch to two arms of the closed ring, and then converge to the lower left corner of the ring, which means that mode f_1 represents a typical dipole resonance. Meanwhile, the surface currents on the metal ground plane, shown in Figure 3b, are reversed, and circulating current loops are formed because the current on two metal layers are anti-parallel, so the magnetic response is excited.

Similarly, for mode f_2, the electric response is excited by surface currents on the metal pattern that flow along two arms of the closed ring, forming a dipole resonance (Figure 3c). However, compare with mode f_1, the surface currents on the closed ring in mode f_2 diverge from the lower right corner and converge to the upper left corner. According to results presented in Figure 3d, the magnetic response of mode f_2 is also excited by circulating currents between two metal layers. In the case of mode f_3, the surface currents are mainly concentrated on the connecting bar between a circular patch and a closed ring (Figure 3e), and mode f_3 represents a dipole resonance that mainly depends on the connecting bar dimensions.

In order to demonstrate the absorption mechanism, the power loss density in the dielectric layer and the ohmic losses at resonator surface for mode $f_1 - f_3$ were determined, and the obtained results are illustrated in Figures 4 and 5, respectively. Dielectric losses of the absorber are mainly concentrated in areas with a strong electric field, while the ohmic losses at resonator surface are determined by surface currents. In addition, it has been observed that the power losses in the dielectric layer are more than dissipated on the resonator surface, and the polyimide film has a very important role in the absorption of the incident waves.

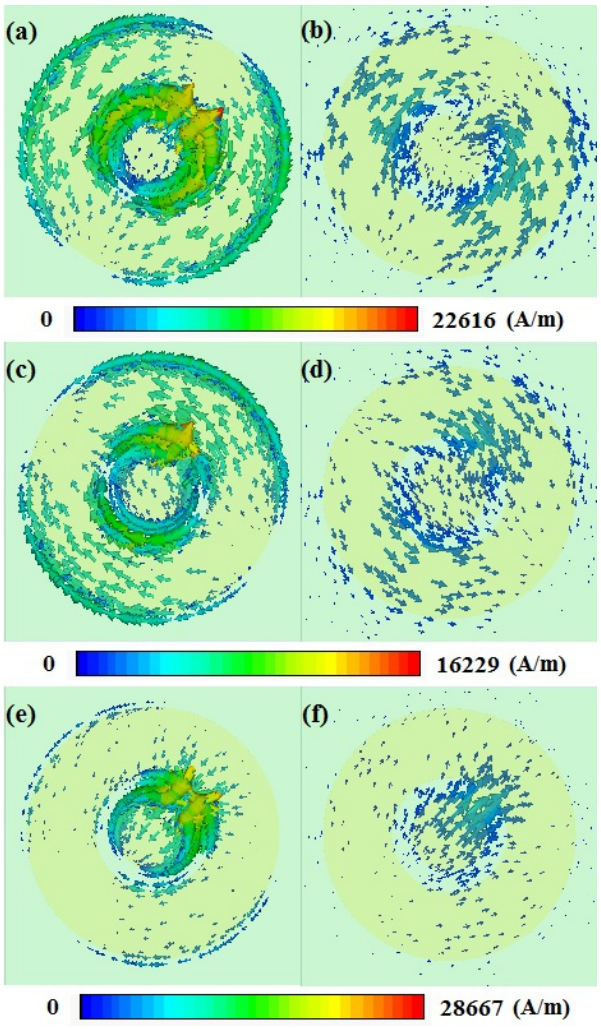

Figure 3. Simulated surface current distribution on (**a**) a metal pattern at 92.4 GHz; (**b**) a metal ground plane at 92.4GHz; (**c**) a metal pattern at 102.0 GHz; (**d**) a metal ground plane at 102.0 GHz; (**e**) a metal pattern at130.1 GHz and (**f**) a metal ground plane at 130.1 GHz.

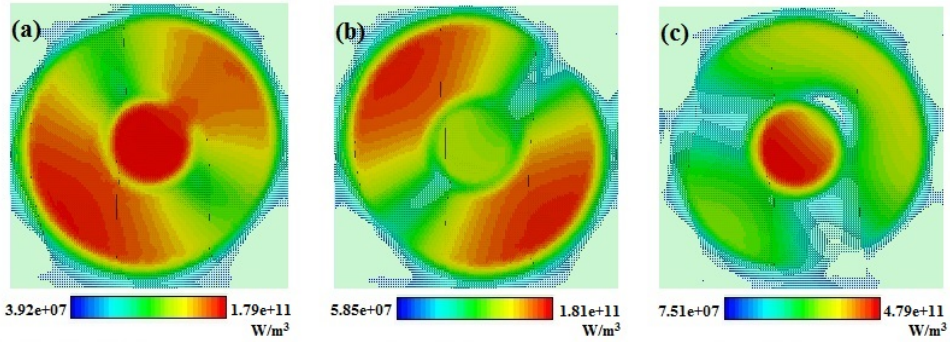

Figure 4. Distribution of dielectric power losses on polyimide film at (**a**) 92.4 GHz; (**b**) 102.0 GHz, and (**c**) 130.1 GHz.

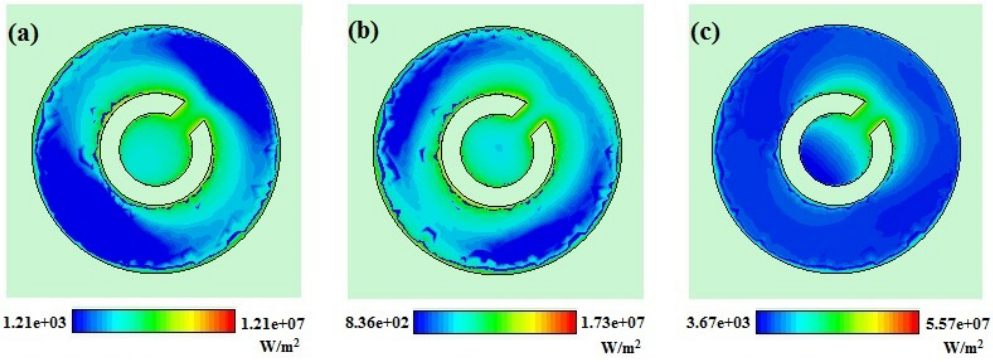

Figure 5. Distribution of ohmic losses on resonator surface at (**a**) 92.4 GHz; (**b**) 102.0 GHz and (**c**) 130.1 GHz.

4. MA Absorption Dependence on the Wave Incident Angle and Polarization

The absorption characteristics of the proposed structure for oblique incident wave with TE polarization were simulated, and the obtained results are shown in Figure 6a. During the calculation, *E*-field was in the *x*-direction, and *H*-field and wave propagation directions varied simultaneously for angle θ.As shown in Figure 6a, when the oblique incident angle increases from 0 to 60°, the absorption peaks at the three resonance frequencies are about 90% or greater, which is caused by a resonator structure, wherein for TE polarization a strong electric resonance can be excited with a relatively small field strength.

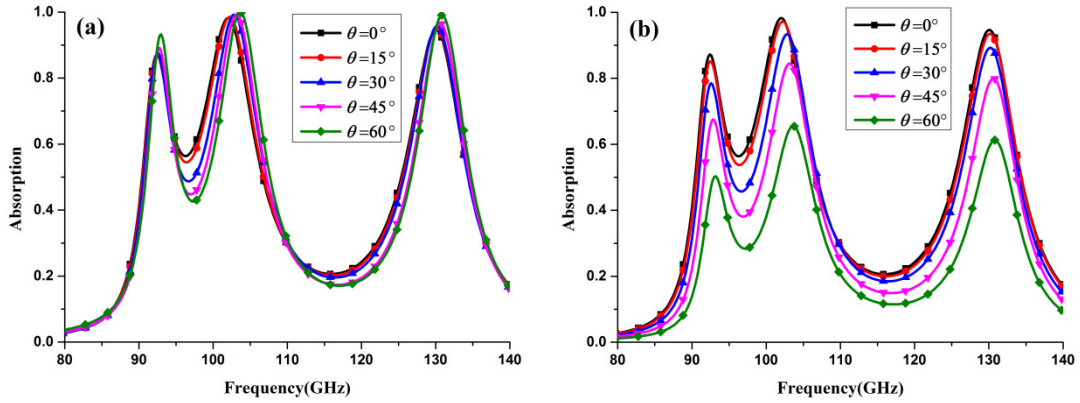

Figure 6. Simulated responses of the structure for different incident angles θ for (**a**) the TE-polarized wave and (**b**) the TM-polarized wave.

For the TM-polarized wave, whose *H*-field is in the *x*-direction, the absorption characteristics for the oblique incident wave were also simulated, and the obtained results are shown in Figure 6b. However, as can be seen in Figure 6b, when the incident angle increases, the absorption characteristic for TM-polarized oblique incidence deteriorates rapidly at all resonance modes.

Nonetheless, we were focused on absorption characteristics for different polarization angles for the normal incident wave. For TE and TM polarization, *E*-field changes for angle φ with respect to the *x*-and *y*-direction, respectively. The simulated responses for TE and TM waves for different polarization angles are presented in Figure 7a,b, respectively. As shown in Figure 7a, for resonant modes f_1 and f_3, the absorption is high when φ is in the range 0–45°. However, the resonance of mode f_2 decreases gradually when φ changes from 0 to 45°. According to results presented in Figure 7a, it can be concluded that the resonance of mode f_2 vanishes at φ = 45° because the surface current on the resonator surface in mode f_2 (Figure 3c) mainly flows perpendicularly to the direction of the electric field vector. Therefore, the electric response cannot be excited.

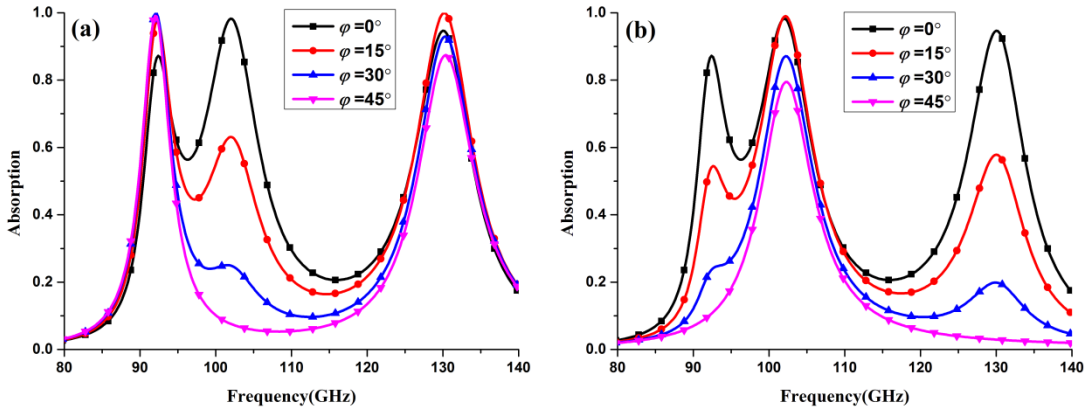

Figure 7. Simulated absorption characteristic of the proposed structure for different polarization angles φ for (**a**) the TE-polarized wave and (**b**) the TM-polarized wave.

Similarly, when TM polarization angle is changed, the absorption peaks for mode f_2 are above 80%, while the absorptivities of mode f_1 and f_3 decrease gradually when φ changes from 0 to 45°. Therefore, the proposed structure provides both single-band and multi-band absorption for different polarization angles.

5. Experimental Results

The MA was fabricated using standard photolithography. Firstly, the copper with a thickness of 0.5 μm was deposited on the bottom surface of the polyimide film. Then, the photolithography was used to define the metallic patterned resonator at the top film surface. Lastly, the copper was evaporated, and a metal lift-off process was used to complete the pattern transfer. The fabricated sample composed by 18×18 unit-cells with a dimension of 1.5 cm×1.5 cm is displayed in Figure 8.

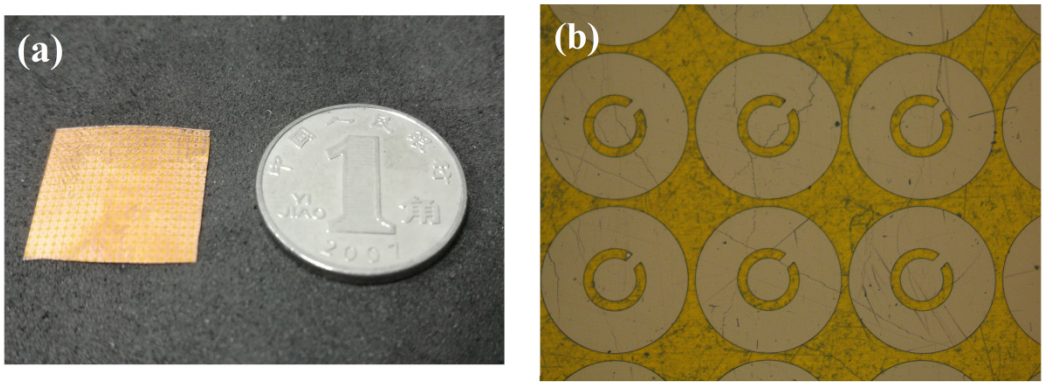

Figure 8. Fabricated metamaterial absorber: (**a**) real size; (**b**) enlarged portion.

The free space measurement method was adopted in the experiment. A pair of horn antennas were connected to the Agilent N5224A vector network analyzer (Agilent Technologies Inc, Santa Clara, CA, USA) via VNA extenders VDI VNAX600 (Virginia Diodes Inc, Charlottesville, VA, USA) that were used for frequency range 90–140 GHz. In this case, one antenna acted as a transmitting antenna and other as a receiving antenna. In order to avoid the reflections from the environment, the calibration was performed as follows. The reflections from an identical copper plate, which acts as an ideal reflector, were firstly measured. Then, the actual reflections from the sample were calculated by comparison of the reflection from the structure and the reflection from the copper plate. It should be noted that, for the given sample dimensions, a minimum far-field distance of 40 cm must be met. Moreover,

the measurement of responses for different incident angles has not been carried out due to the large scattering of this finite sample at wide incident angles [30].

The measured MA absorption for various polarization angles (φ) for both TE-polarized and TM-polarized normal incident waves is presented in Figure 9. For TE-polarization, a dual-band absorption is achieved for a polarization angle of 45°. However, only one absorption peak with absorptivity of above 70% is achieved for polarization angle of 45° in the case of TM-polarized incident wave, which is in agreement with the simulated results.

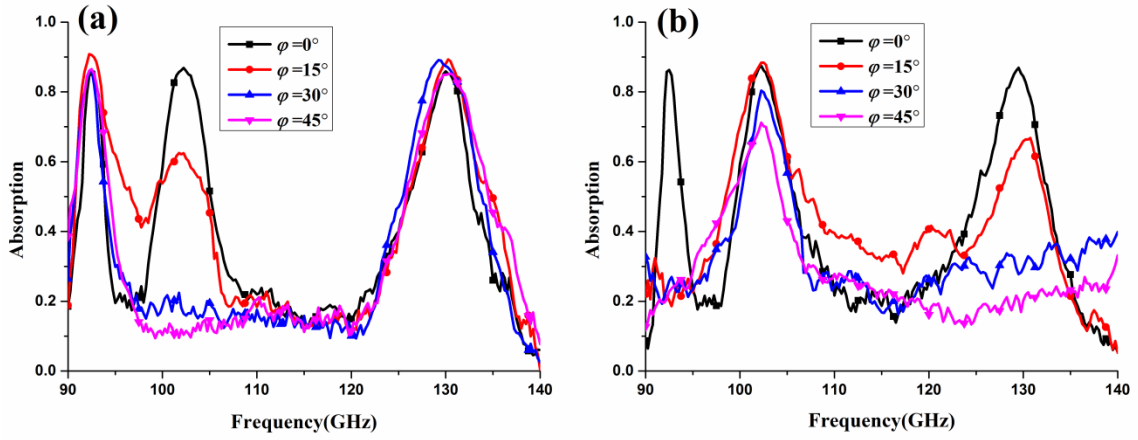

Figure 9. Measured MA absorption for different polarization angles for (**a**) the TE-polarized wave and (**b**) the TM-polarized wave.

6. Conclusions

A simple design of a polarization-dependent frequency-selective metamaterial absorber based on a circular patch with a C-shaped slot is presented. In contrast to previous studies on compression of multi resonators, in the proposed design, a multi-band absorption is obtained using a simple resonant structure. Furthermore, changing the polarization angle of the incident wave, a triple-band, a dual-band, and a single-band absorptions can be achieved, which is required in the polarization-dependent detection. In order to demonstrate the absorption mechanism, the electric field distribution, the surface current distribution, and the power-loss distributions were obtained. The proposed design was verified both by simulations and experiments, which were performed using the free space measurement method. A good agreement between simulated and measured results was achieved, which proves a high absorption performance of the proposed MA.

Acknowledgments: This work was supported by the National Natural Science Foundation of China (No. 51607050) and the National Defense Pre-Research Foundation of China (Grant No. 6140239010106).

Author Contributions: Guangsheng Deng and Zhiping Yin conceived and wrote the paper; Tianyu Xia and Yong Fang performed the experiments; Jun Yang guided the experimental design and analyzed the data.

Conflicts of Interest: The authors declare no conflict of interest.

References

1. Smith, D.; Pendry, J.; Wiltshire, M. Metamaterials and negative refractive index. *Science* **2004**, *305*, 788–792. [CrossRef] [PubMed]
2. Chen, H.T.; Padilla, W.J.; Zide, J.M.; Gossard, A.C.; Taylor, A.J.; Averitt, R.D. Active terahertz metamaterial devices. *Nature* **2006**, *444*, 597–600. [CrossRef] [PubMed]
3. Poddubny, A.; Iorsh, I.; Belov, P.; Kivshar, Y. Hyperbolic Metamaterials. *Nat. Photonics* **2013**, *7*, 948–957. [CrossRef]
4. Chen, H.S.; Wu, B.I.; Zhang, B.; Kong, J.A. Electromagnetic wave interactions with a metamaterial cloak. *Phys. Rev. Lett.* **2007**, *99*, 063903. [CrossRef] [PubMed]

5. Valentine, J.; Zhang, S.; Zentgraf, T.; Ulin-Avila, E.; Genov, D.A.; Bartal, G.; Zhang, X. Three-dimensional optical metamaterial with a negative refractive index. *Nature* **2008**, *455*, 376–379. [CrossRef] [PubMed]
6. Kaina, N.; Lemoult, F.; Fink, M.; Lerosey, G. Negative refractive index and acoustic superlens from multiple scattering in single negative metamaterials. *Nature* **2015**, *525*, 77–81. [CrossRef] [PubMed]
7. Landy, N.; Sajuyigbe, S.; Mock, J.; Smith, D.; Padilla, W. Perfect metamaterial absorber. *Phys. Rev. Lett.* **2008**, *100*, 207402. [CrossRef] [PubMed]
8. Yin, S.; Zhu, J.F.; Xu, W.D.; Jiang, W.; Yuan, J.; Yin, G.; Xie, L.J.; Ying, Y.B.; Ma, Y.G. High-performance terahertz wave absorbers made of silicon-based metamaterials. *Appl. Phys. Lett.* **2015**, *107*, 073903. [CrossRef]
9. Huang, L.; Chowdhury, D.R.; Ramani, S.; Reiten, M.T.; Luo, S.N.; Taylor, A.J.; Chen, H.T. Experimental demonstration of terahertz metamaterial absorbers with a broad and flat high absorption band. *Opt. Lett.* **2012**, *37*, 154–156. [CrossRef] [PubMed]
10. Shi, C.; Zang, X.F.; Wang, Y.Q.; Chen, L.; Cai, B.; Zhu, Y.M. A polarization-independent broadband terahertz absorber. *Appl. Phy. Lett.* **2014**, *105*, 031104. [CrossRef]
11. Zhu, W.R.; Huang, Y.J.; Rukhlenko, I.D.; Wen, G.J.; Premaratne, M. Configurable metamaterial absorber with pseudo wideband spectrum. *Opt. Express* **2012**, *20*, 6612–6621. [CrossRef] [PubMed]
12. Wang, B.X.; Zhai, X.; Wang, G.Z.; Huang, W.Q.; Wang, L.L. Design of a Four-Band and Polarization-Insensitive Terahertz Metamaterial Absorber. *IEEE Photonics J.* **2015**, *7*, 4600108. [CrossRef]
13. Faraji, M.; Morawej-Farshi, M.K.; Yousefi, L. Tunable THz perfect absorber using graphene-based metamaterials. *Opt. Commun.* **2015**, *355*, 352–355. [CrossRef]
14. Zhu, J.F.; Ma, Z.F.; Sun, W.J.; Ding, F.; He, Q.; Zhou, L.; Ma, Y.G. Ultra-broadband terahertz metamaterial absorber. *Appl. Phys. Lett.* **2014**, *105*, 021102. [CrossRef]
15. He, X.J.; Yan, S.T.; Ma, Q.X.; Zhang, Q.F.; Jia, P.; Wu, F.M.; Jiang, J.X. Broadband and polarization-insensitive terahertz absorber based on multilayer metamaterial. *Opt. Commun.* **2015**, *340*, 44–49. [CrossRef]
16. Shrekenhamer, D.; Chen, W.C.; Padilla, W.J. Liquid Crystal Tunable Metamaterial Absorber. *Phys. Rev. Lett.* **2013**, *110*, 177403. [CrossRef] [PubMed]
17. Zhang, Y.; Feng, Y.; Zhu, B. Graphene based tunable metamaterial absorber and polarization modulation in terahertz frequency. *Opt. Express* **2014**, *22*, 22743–22752. [CrossRef] [PubMed]
18. Yahiaoui, R.; Guillet, J.P.; de Miollis, F.; Mounaix, P. Ultra-flexible multiband terahertz metamaterial absorber for conformal geometry applications. *Opt. Lett.* **2013**, *38*, 4988–4990. [CrossRef] [PubMed]
19. Yahiaoui, R.; Tan, S.Y.; Cong, L.Q.; Singh, R.; Yan, F.P.; Zhang, W.L. Multispectral terahertz sensing with highly flexible ultrathin metamaterial absorber. *J. Appl. Phys.* **2015**, *118*, 083103. [CrossRef]
20. Yahiaoui, R.; Hanai, K.; Takano, K.; Nishida, T.; Miyamaru, F.; Nakajima, M.; Hangyo, M. Trapping waves with terahertz metamaterial absorber based on isotropic Mie resonators. *Opt. Lett.* **2015**, *40*, 3197–3200. [CrossRef] [PubMed]
21. Singh, P.K.; Korolev, K.A.; Afsar, M.N.; Sonkusale, S. Single and dual band 77/95/110 GHz metamaterial absorbers on flexible polyimide substrate. *Appl. Phys. Lett.* **2011**, *99*, 264101. [CrossRef]
22. Zhou, W.; Wang, P.; Wang, N.; Jiang, W.; Dong, X.; Hu, S. Microwave metamaterial absorber based on multiple square ring structures. *AIP Adv.* **2015**, *5*, 117109. [CrossRef]
23. Hokmabadi, M.P.; Wilbert, D.S.; Kung, P.; Kim, S.M. Polarization-Dependent, Frequency-Selective THz Stereometamaterial Perfect Absorber. *Phys. Rev. Appl.* **2014**, *1*, 044003. [CrossRef]
24. Hu, F.R.; Zou, T.B.; Quan, B.G.; Xu, X.L.; Bo, S.H.; Chen, T.; Wang, L.; Gu, C.Z.; Li, J.J. Polarization-dependent terahertz metamaterial absorber with high absorption in two orthogonal directions. *Opt. Commun.* **2015**, *332*, 321–326. [CrossRef]
25. Wang, B.X.; Wang, G.Z.; Sang, T. Simple design of novel triple-band terahertz metamaterial absorber for sensing application. *J. Phys. D Appl. Phys.* **2016**, *49*, 165307. [CrossRef]
26. Mao, Z.W.; Liu, S.B.; Bian, B.R.; Wang, B.Y.; Ma, B.; Chen, L.; Xu, J.Y. Multi-band polarization-insensitive metamaterial absorber based on Chinese ancient coin-shaped structures. *J. Appl. Phys.* **2014**, *115*, 204505. [CrossRef]
27. Arezoomanda, A.S.; Zarrabib, F.B.; Heydaria, S.; Gandjic, N.P. Independent polarization and multi-band THz absorber base on Jerusalem cross. *Opt. Commun.* **2015**, *352*, 121–126. [CrossRef]
28. Bhattacharyya, S.; Ghosh, S.; Srivastava, K.V. Triple band polarization-independent metamaterial absorber with bandwidth enhancement at X-band. *J. Appl. Phys.* **2013**, *114*, 094514. [CrossRef]

29. Hu, F.R.; Wang, L.; Quan, B.G.; Xu, X.L.; Li, Z.; Wu, Z.A.; Pan, X.C. Design of a polarization insensitive multiband terahertz metamaterial absorber. *J. Phys. D Appl. Phys.* **2013**, *46*, 195103. [CrossRef]
30. Álvarez, H.F.; Gómez, M.E.; Las-Heras, F. Angular stability of metasurfaces: Challenges regarding reflectivity measurements. *IEEE Antennas Propag. Mag.* **2016**, *58*, 74–81. [CrossRef]